Empirical evidences of a common multifractal signature in economic, biological and physical systems

Oriol Pont, Antonio Turiel, Conrad J. Perez-Vicente

Physica A 388 (2009) 2025–2035

Empirical evidences of a common multifractal signature in economic, biological and physical systems

Oriol Pont [a,*], Antonio Turiel [b], Conrad J. Pérez-Vicente [a]

[a] *Departament de Física Fonamental. Universitat de Barcelona. Diagonal, 647. 08028 Barcelona, Spain*
[b] *Institut de Ciències del Mar, CSIC. Passeig Marítim de la Barceloneta, 37-49. 08003 Barcelona, Spain*

ARTICLE INFO

PACS:
47.53.+n
89.75.Da
47.11.+j

ABSTRACT

Recent developments in microcanonical multifractal formalism have lead to a sensible improvement in the numerical techniques for the determination of the multifractal characteristics of real signals. With the aid of these techniques, we have found empirical evidence of a common multifractal signature in six very different systems, ranging from stock market time series to sea surface temperature records. These systems are not only found to be multifractal, but their singularity spectra are coincident. We propose an explanation of this striking coincidence in terms of a cascade process and analyze its consequences.

1. Introduction

Fractality, a concept coined more than forty years ago, has been used as a standard strategy to describe self-similar systems. Later on, the study of turbulence favored the introduction of multifractals: coordinated ensembles of fractals, organized in a hierarchical way. Multifractals are more flexible, more adapted to fully describe the structure of many physical systems, and evidence grows on their ubiquitous presence in nature. Starting from the study of turbulent flows [1–7], for which the theory was first developed, multifractality has been reported in many other systems, some of them completely unrelated to turbulence. These include natural images [8,9], stock market series [10–17], human gait [18,19], the heliospheric magnetic field [20], network traffic [21], phytoplankton distribution in oceans [22], rainfall distribution [23–25], sea surface temperature [26,27], heartbeat dynamics [28,29], distribution of chemical fields [30,31], cloud structure [32,33], many different geophysical fields [34,35] and a long etc.

A multifractal is a scale-free (scale invariant) system. This means that the statistical properties of small regions are the same as those of the whole system: they are self-similar. Self-similarity is also a classical fingerprint of fractal sets, but multifractals have a much richer structure. The main difference between fractals and multifractals is that, in a fractal, to describe how a variable behaves under changes of scale, only one parameter – the fractal dimension – is needed. In contrast, a multifractal is formed by a hierarchy of multiple fractal sets, so all their fractal dimensions are required to characterize how the system evolves under changes of scale. Therefore, the key quantity defining a multifractal is the collection of all its fractal dimensions: the *singularity spectrum*.

* Corresponding author. Tel.: +34 934039206; fax: +34 934021149.
E-mail addresses: oriol@ffn.ub.es (O. Pont), turiel@icm.csic.es (A. Turiel), conrad@ffn.ub.es (C.J. Pérez-Vicente).

The hierarchical organization of a multifractal structure has been related to the existence of cascade processes. Had this concept either a real basis in terms of physical observables or an effective one in terms of hidden variables their relevance is capital to give insight on the dynamics of some physical systems. The implications of these ideas are so deep that some authors have claimed the existence of universal multifractals [24].

The classical approach to characterize multifractality in experimental data is to apply the Canonical Multifractal Formalism (CMF) [1,36,37,3,38]. In this approach, the fractal dimensions of the different fractal components of the system are indirectly evaluated using some statistical and geometrical reasoning [39]. For that, the order-p moments of an appropriate variable (structure functions) are evaluated and its behavior under changes of scale are characterized with the so-called scaling exponents τ_p. Then, under some assumptions on the homogeneity of the underlying multifractal geometry, the singularity spectrum is derived using Parisi and Frisch's formula [39]. The main advantage of this approach lies in its simplicity; besides, it is very useful when data are obtained in a fragmentary way and so a geometrical processing is not possible. The main drawback is that the canonical approach is very demanding of data, what limits the range of the singularity spectrum that can be retrieved in practical situations. Moreover, it is prone to be affected by other processing issues (see Ref. [40] for a discussion on the topic).

An alternative approach to the study of multifractal properties of real signals is the Microcanonical Multifractal Formalism (MMF). Although the roots of MMF can be tracked in the works by Chhabra et al. almost twenty years ago [41], they have not been set to efficiently process real signals up to recently [9,42,27,43]. In MMF, signal processing is geometrical instead of statistical, and the goal is to obtain the local scaling exponents. These exponents identify the fractal components from which the singularity spectrum can be derived directly. MMF analysis methods are much less demanding in data than their CMF counterparts, and in addition they allow the study of the geometrical properties of signals, what can be used to compress them [44], to infer their future evolution [14,15], and to characterize the underlying forces driving their dynamics [26,25].

In this paper we characterize the multifractal properties of six ensembles of signals obtained from very different systems (see description in Appendix A). In Section 2 we discuss on how their statistical properties can be related to an underlying multifractal structure. Then, we apply MMF to obtain the associated singularity spectra and we see that the six resulting spectra are related (Section 3). This raises a question about a possible common effective mechanism giving rise to the observed similarity. We propose a possible mechanism based on an effective cascade process shared by all the systems under study (Section 4). Finally, in Section 5 we discuss the results in the perspective of defining canonical classes of multifractal systems.

Note on the reproducibility of the empirical evidences shown in this paper

The study presented in this paper is not just a simple empirical analysis of some multifractal signals, since the methodology used throughout has a very solid theoretical support. It is a direct implementation of a formalism (MMF) that reveals with high accuracy the complex structure of multifractal signals. Before tackling some theoretical considerations, let us remark that to favor reproducibility of our results, an open-source C program, capable of obtaining the singularity exponents of a given signal, is at the disposal of any interested reader at: http://www.icm.csic.es/oce/people/turiel/SUPP_INFO/MF-analyzer.html

2. Statistical signature of multifractality

2.1. Intermittency

There is a basic common feature in all multifractal signals coming from real-world systems: intermittency. Intermittent signals are close to a reference value for long times and suddenly they undergo sharp, short-lived changes [34]. Thus, when intermittency is present, histograms of the derivative of the signal have a small mode (most probable value) and a slow-decaying tail. To illustrate this concept with real data, let us consider six ensembles of 1D and 2D physical, biological and economic signals of very different nature, known to be multifractal. These are: Ensemble A: stock market series; Ensemble B: currency exchange series; Ensemble C: sea temperature series; Ensemble D: sea temperature 2D maps; Ensemble E: natural images; and Ensemble F: turbulent flow 2D maps. A representative signal of each ensemble is shown in the left-hand-side of Fig. 1. Details on the data are exposed in Appendix A. These datasets have been originated from very different physical processes and so one can expect large differences in their statistical properties, as the histograms in the center of Fig. 1 reveal. Nevertheless, even if the signals are very different, the histograms of the absolute values (moduli for 2D) of the derivatives (gradients for 2D) are qualitatively similar (see the right-hand-side histograms of Fig. 1). This coincidence reveals that all those systems are intermittent, at least in the probabilistic sense enunciated above. As we will see later, the similarity of these systems can be expressed in a more quantitative way.

Although revealing, histograms of gradients are not appropriate to describe multifractal scaling properties. Gradients are dimensional and scale-dependent: they are estimated at a given resolution and depend on the local amplitude of the signal. We need a different approach to invariantly analyze the multifractal signals and the key tool to carry out this analysis is MMF [41,9,42,27,43].

According to MMF, a scalar signal $s(\vec{x})$ (where $\vec{x}$ is the position vector) is multifractal if it can be characterized by an underlying hierarchy of scale-invariant fractal components. Each fractal component of the signal transforms differently

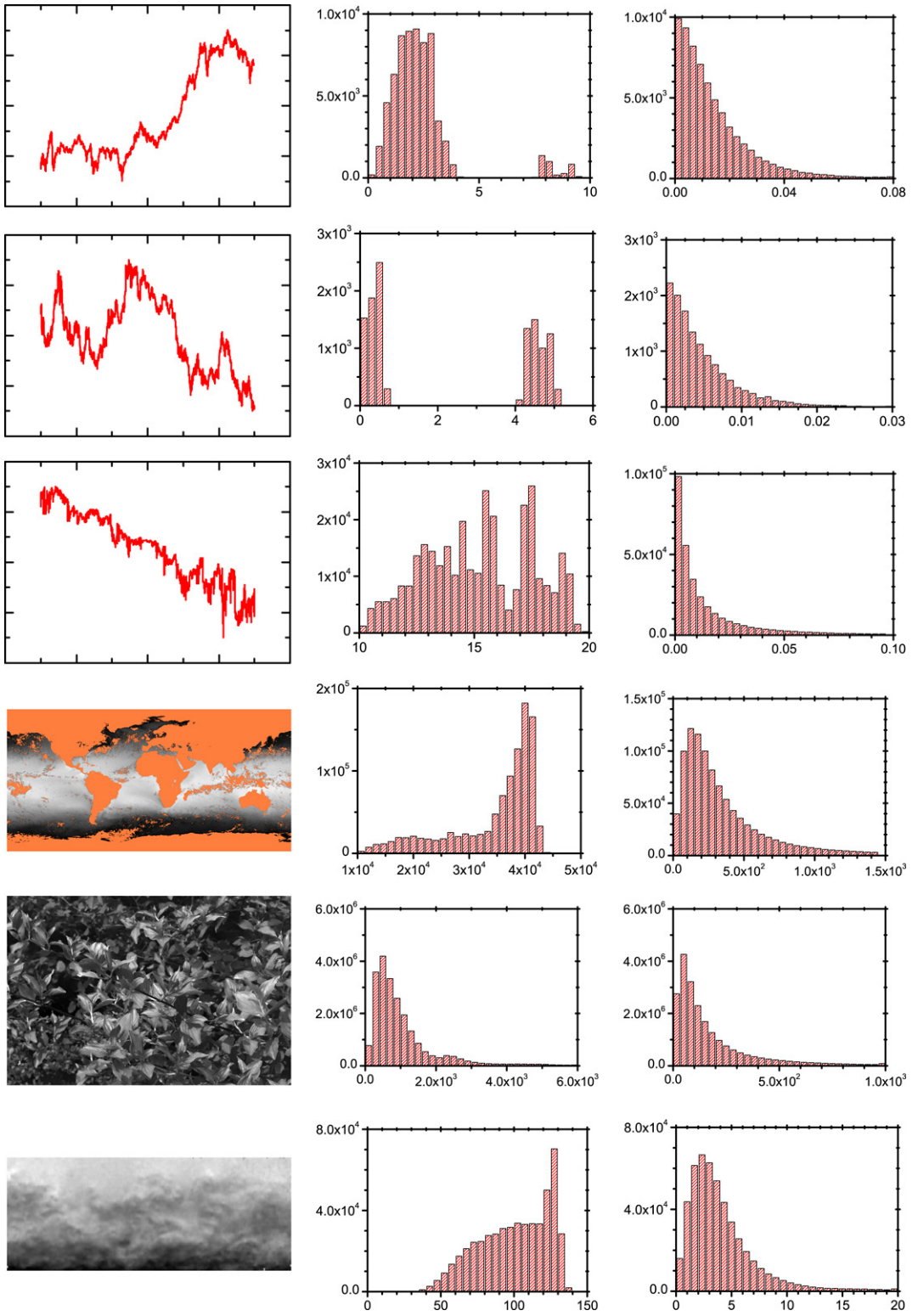

Fig. 1. Left: A representative signal from each ensemble; Center: Histograms of the signal values; Right: Histograms of the derivative variables (absolute value of the derivative for 1D signals, modulus of the gradient for 2D signals). Ensembles from top to bottom: (A) 20 quotation time series from the Spanish stock market from 1990 to 2000, sampled daily. (B) 9 currency exchange rate time series from 1992 to 1997, sampled daily. (C) 6 three-month sea temperature time series, sampled at a 12-min rate. Data were obtained from a mooring settled in front of the Ebro river delta [45,46]. (D) Two weekly averages of Sea Surface Temperature images, corresponding to the week 2–9 February, 2003 and the week 14–21 April, 2004. The studied area goes from 34° W to 8.5° E, and from 45° S to 2.5° S. (E) 14 natural images from Hans van Hateren's web database [47]. (F) 50 2D maps of high-Reynolds velocity fields generated in a wind tunnel [48]. The velocities were estimated using the Maximum Cross Correlation Method [49] on a dispersed colorant.

under changes of scale, following a power-law behavior with an exponent that varies from one component to another. In fact, decomposing a multifractal into fractal components means that each signal point is associated to one and only one fractal component. So that, each point $\vec{x}$ has a *singularity exponent* $h(\vec{x})$ associated, and each singularity exponent value h defines a fractal component $\mathcal{F}_h$, i.e., the fractal components are level sets of the function $h(\vec{x})$: $\mathcal{F}_{h_0} = \{\vec{x} \text{ such that } h(\vec{x}) = h_0\}$. Let us now clarify these concepts in detail.

2.2. Singularity analysis

The singularity exponent $h(\vec{x})$ of a function characterizes how this function behaves locally, giving a dimensionless, scale-invariant measure of the degree of regularity around a given point $\vec{x}$. The simplest way to obtain the singularity exponent is by means of the Hölder exponent, when this quantity can be calculated. Let us denote by $s(\vec{x})$ the value of the function at a point $\vec{x}$; for any radius r small enough, the Hölder exponent $h(\vec{x})$ is evaluated according to the following expression:

$$\frac{1}{r}|s(\vec{x}+\vec{r}) - s(\vec{x})| = \alpha(\vec{x})r^{h(\vec{x})} + o(r^{h(\vec{x})}) \tag{1}$$

where the notation $o(r^{h(\vec{x})})$ means a quantity that decreases to zero faster than $r^{h(\vec{x})}$ when r goes to 0, $h(\vec{x})$ is the singularity exponent (Hölder exponent, in this context) and $\alpha(\vec{x})$ is a dimensional, signal-dependent amplitude prefactor. From the expression above, it is evident that the singularity exponent controls the approaching to the point $\vec{x}$ when the radius r decreases. According to Eq. (1), the gradient estimated at a small discrete scale r_0 behaves as $|\nabla s|(\vec{x}) \sim \alpha(\vec{x})r_0^{h(\vec{x})}$ and consequently the singularity exponent $h(\vec{x})$ roughly corresponds to:

$$h(\vec{x}) \sim \frac{\log|\nabla s|(\vec{x})}{\log r_0} \tag{2}$$

when r_0 is small enough. The symbol $\sim$ means that both sides asymptotically equal as $r_0 \to 0$.

When real data are processed, the situation is a bit more complicated. The presence of long-range correlations can mask the value of the singularity exponent and so the signal must be filtered by means of wavelet projections [3,38,9]. The use of wavelet projections is also convenient in order to diminish the influence of acquisition and sampling noises, and to provide a stable interpolation scheme in a continuous range of scales [9]. For a given wavelet Ψ, the wavelet projection of $|\nabla s|$ at the point $\vec{x}$ and scale r is defined as:

$$T_\Psi|\nabla s|(\vec{x}, r) \equiv \int \mathrm{d}\vec{y}|\nabla s|(\vec{y})\frac{1}{r^d}\Psi\left(\frac{\vec{x}-\vec{y}}{r}\right) \tag{3}$$

where d is the dimensionality of the signal (the dimension of the signal domain: $d = 2$ for images, $d = 1$ for series). If the signal s has a Hölder exponent $h(\vec{x})$ at a point $\vec{x}$, Eq. (1), it follows that the wavelet projections $T_\Psi|\nabla s|(\vec{x}, r)$ of the modulus of the gradient $|\nabla s|$ on any appropriate wavelet Ψ present the same scaling, namely:

$$T_\Psi|\nabla s|(\vec{x}, r) = \alpha_\Psi(\vec{x})r^{h(\vec{x})} + o(r^{h(\vec{x})}). \tag{4}$$

Wavelet projections allow generalizing of the concept of Hölder exponent when long-range correlations are present; in that case, we will talk about singularity exponents. Different wavelets can be used to obtain the singularity exponents [9]. See also Ref. [43] for a discussion on the requirements on the wavelet in order to verify Eq. (4).

2.3. Singularity spectrum

A signal $s(\vec{x})$ is called multifractal if a singularity exponent $h(\vec{x})$ can be assigned at every point $\vec{x}$ (following Eq. (4)), also if the level sets of $h(\vec{x})$ – the fractal components – are fractal.

Since each fractal component $\mathcal{F}_h$ is fractal, it can be characterized by its fractal dimension $D(h)$ [50], and the whole set of fractal dimensions $D(h)$ forms the so-called singularity spectrum. The singularity spectrum plays a central role in the description of the scaling properties of a multifractal system [38], because it is directly linked to the statistical properties of the system through the famous Parisi–Frisch's formula [39]. In fact, the empirical histogram of singularities $\rho(h)$, when the singularity exponents are evaluated at the resolution scale r_0, has a simple relation with the singularity spectrum [50]:

$$\rho(h) = A_\rho r_0^{d-D(h)} \tag{5}$$

where d is the dimension of the signal domain, as before.

If the signal has total support (i.e., non-fractal, the common case with real signals) then the support of the function $h(\vec{x})$ is also total and has dimension d. So there must exist a fractal component of such a dimensionality, i.e., there is a value of singularity exponent h_1 such that $D(h_1) = d$, and this value necessarily corresponds to the mode (the most probable value) of $\rho(h)$ [38,9,40]. Therefore, when the histogram is normalized by its mode, the proportionality constant A_ρ is removed and

Table 1
Percentage of points that have a regression coefficient higher than 0.999 in the regression performed to retrieve the singularity exponents. The ranges of scales used go from 1 point to about 10% of the linear size of the signal. 20 regression points have been log-uniformly sampled in this range. The results were obtained using our program, and the wavelet used for this analysis is a Gaussian function; other wavelets give similar results.

Ensemble	A	B	C	D	E	F
% good regression points	99.7%	99.4%	99.7%	99.4%	99.7%	99.6%

so we can retrieve the dimensionless, scale-invariant quantity $D(h) - d$ in the way:

$$D(h) - d = -\frac{\log\left(\frac{\rho(h)}{\rho(h_1)}\right)}{\log r_0} \tag{6}$$

for any resolution scale r_0 at which the singularity exponents are evaluated. $D(h) - d$ is called *reduced singularity spectrum*, and it is independent of the dimensionality d.

2.4. Definition of MMF

So far, we have introduced the two main elements of MMF (singularity analysis and singularity spectrum). Let us formalize the requirements on a real signal in order to accept that MMF holds for it:

(i) For any point $\vec{x}$, Eq. (4) is verified over a large enough range of scales.
(ii) The distribution of singularity exponents at any valid scale r_0 follows Eq. (5) with the same curve $D(h)$.
(iii) The curve $D(h)$ derived from Eq. (6) is convex.

These conditions and what they imply are discussed in detail in Ref. [42,27,43]. For the context of this paper, we will just verify the extent of validity of conditions (i), (ii) and (iii) for the datasets we have analyzed.

The main virtue of MMF is that it allows an explicit geometrical determination of the fractal components [9]. Hence, the retrieval of the singularity spectrum $D(h)$ by means of Eq. (6) is more direct than in classical multifractal techniques and less demanding in data size [40].

3. Experimental results

3.1. Validity of MMF

In order to apply MMF on real data, the three requirements presented in Section 2.4 must be fulfilled. The first step is to verify the validity of MMF for the datasets under study, even in those cases where it has already been reported such as in ensembles A, B, D and E (see Ref. [14,17,27,9]). On the contrary, no dedicated study exists for ensembles C and F. Nevertheless, being thermodynamical variables in turbulent flows they can reasonably be expected to be multifractal [5].

Regarding condition (i), we must check the range over which Eq. (4) can be considered to fit our data, taking into account that noise, discretization and finite-size effects impose experimental bounds to the validity of this equation. As we are interested in retrieving the singularity exponent $h(\vec{x})$ at each point $\vec{x}$, we will perform a log-log regression of Eq. (4) vs. r; the slope of the logarithmic regression is $h(\vec{x})$. We consider that the local scaling is well verified at a given point and for a range of scales (r_0, r_1) when the regression coefficient is above an adequate threshold. We have seen that all the analyzed signals presented more than 99% of points with a regression coefficient higher than 0.999 for $r_0 = 1$ point and $r_1 = 10\%$ of the system size, with 20 regression points uniformly sampled on the log axis; see Table 1. We thus conclude that condition (i) is well verified.

Regarding condition (ii), we have obtained the singularity spectra (using Eq. (6)) at two different scales, namely the finest possible scale and twice the finest possible scale. In Fig. 2, we present the spectra of all the ensembles as obtained at these two scales, showing that all the spectra coincide to a great extent.

Condition (iii) is just requiring that singularity spectra are convex. All the singularity spectra are convex curves, see Fig. 2, so condition (iii) is also satisfied. Therefore, we conclude that the six datasets verify MMF.

3.2. Comparison of the singularity spectra

In Fig. 3 we show the reduced singularity spectra of the studied ensembles. The reader will notice the remarkable coincidence among all of them regardless their different nature. Besides, reduced singularity spectra disregard the difference of dimensionality and allow us to observe that their multifractal structure is essentially the same. Certainly, this fact explains why gradient histograms presented at the right hand side of Fig. 1 are so similar, but also reveals the existence of a much deeper link between these ensembles.

Nevertheless, in Fig. 3 we can observe some differences between the singularity spectra, which are more evident when the spectra are observed in isolation in Fig. 4. These differences mainly concentrate on the tails of the curves, i.e., the values

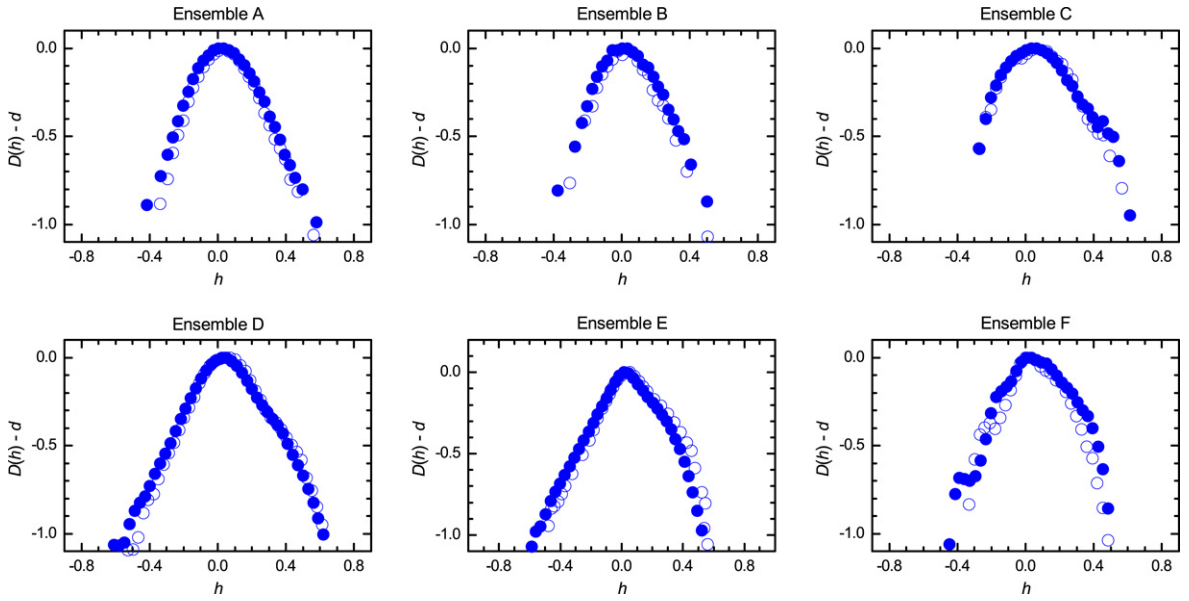

Fig. 2. Reduced singularity spectra of each ensemble (top: A, B and C; Bottom: D, E and F), calculated at the finest possible scale r_0, full circles, and twice the finest scale possible $2r_0$, hollow circles.

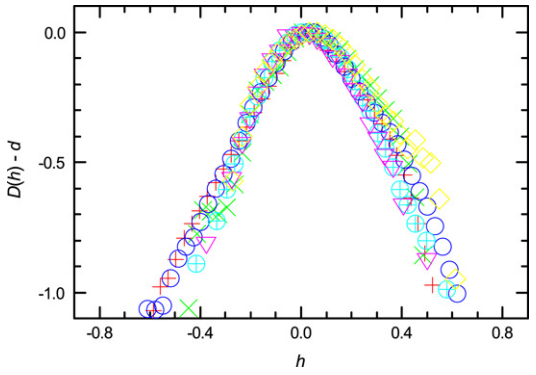

Fig. 3. Reduced singularity spectra obtained for the different ensembles: Ensemble A (⊕), Ensemble B (▽), Ensemble C (◇), Ensemble D (○), Ensemble E (+) and Ensemble F (×).

of h associated to the fractal components of smaller dimension, which in fact correspond to the less probable values of h according to Eq. (5). This is not strange because these values have small probability and the uncertainty in the estimation of $\rho(h)$, and hence in that of $D(h) - d$, is greater for them. In fact, in Ref. [40] a simple method to estimate the uncertainty in the value of $D(h)$ was introduced. In Fig. 4 we show the singularity spectra for the six ensembles in which the error bars are included. As expected, the ensembles with less data points have greater error bars on average. Besides, in all the spectra the tails (less sampled values) also have greater error bars.

We can quantify the degree of mutual closeness among the singularity spectra. Given two reduced spectra, $D_1(h) - d_1$ and $D_2(h) - d_2$, with associated uncertainties $b_1(h)$ and $b_2(h)$, we define their directed weighted average difference $\delta D_{1\to 2}$ as follows:

$$\delta D_{1\to 2} \equiv \sum_{h_n} \frac{|D_1(h_n) - d_1 - D_2(h_n) + d_2|}{b_1(h_n) b_2(h_n)} \Bigg/ \sum_{h_n} \frac{1}{b_1(h_n) b_2(h_n)} \tag{7}$$

where $\{h_n\}$ are the points at which D_1 is sampled in the experimentally obtained singularity spectrum. As the points $\{h_n\}$ are not sampling points of D_2 in general, $D_2(h)$ and $b_2(h)$ are linearly interpolated to evaluate their value at each h_n. In addition, the sum in Eq. (7) is restricted to the values of $\{h_n\}$ in the common range of h values for $D_1(h)$ and $D_2(h)$. Finally, we define the weighted average difference between the two reduced singularity spectra, δD_{12}, as the minimum of the two possible directed weighted average differences,

$$\delta D_{12} \equiv \text{Min}\left(\delta D_{1\to 2}, \delta D_{2\to 1}\right). \tag{8}$$

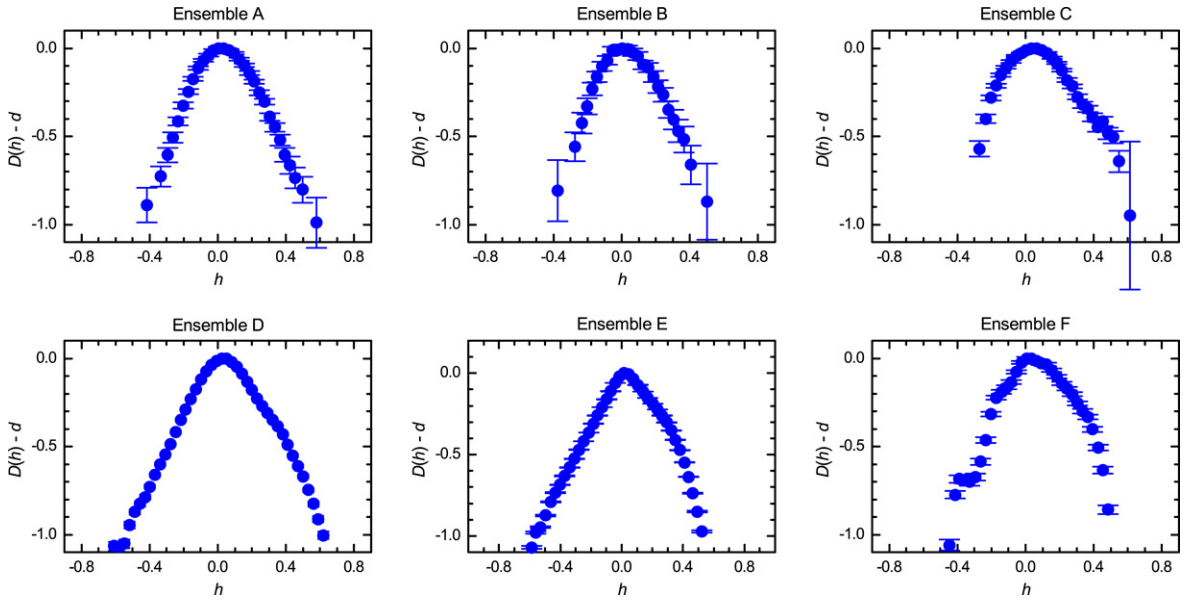

Fig. 4. Reduced singularity spectra of each ensemble (top: A, B and C; Bottom: D, E and F), calculated at the finest possible scale r_0, including the error bars associated to sampling-size uncertainties. The average sizes of the error bars are the following: Ensemble A: 0.12; Ensemble B: 0.11; Ensemble C: 0.06; Ensemble D: 0.05; Ensemble E: 0.02; Ensemble F: 0.06.

Table 2
Directed weighted average differences $\delta D_{i\to j}$, Eq. (7), for the six ensembles.

	A	B	C	D	E	F
A	0	0.01	0.03	0.02	0.04	0.04
B	0.01	0	0.04	0.03	0.05	0.05
C	0.03	0.04	0	0.03	0.07	0.03
D	0.02	0.03	0.03	0	0.03	0.04
E	0.04	0.04	0.06	0.03	0	0.05
F	0.04	0.05	0.03	0.04	0.06	0

In Table 2 we presented the directed weighted average differences between the six ensembles.

We can see that for any couple of ensembles i, j, the two directed weight averages $\delta D_{i\to j}$ and $\delta D_{j\to i}$ are always very similar, differing at most by 0.01. This means that our criterion is reasonably stable and is not affected by the choice of the reference range of values of h. We observe that the greatest weighted average difference corresponds to $\delta D_{CE} = 0.06$, which although important is smaller than the typical error bar in Ensemble C. It is interesting to notice that the deviation between the two spectra seems more important on the right tail. Such a deviation could be due to the difficulties of estimating high values of the singularity exponents, which imply highly regular behavior that can only be properly assessed when rather large scales are considered [40,43]. Concerning the other weighted average differences, they are smaller and compatible with the observed size of the error bars. Hence, we accept that at least in a first approximation the six spectra are coincident.

4. A common effective mechanism: Reconstruction

Fractals are strongly linked to systems undergoing critical transitions. Close to the critical set, all the scaling properties of the system are characterized by the so-called *critical exponent*; in turn, the critical set itself is a fractal set, univocally associated to that critical exponent. Close to the transition, all physical systems with the same critical exponents behave identically, regardless particular microscopic details of the underlying dynamics. That is, these systems belong to the same universality class. The study of critical systems is then reduced to the study of their associated universality classes [51]. For multifractals, one can extend the idea and assume that systems with the same singularity spectrum belong to the same universality class, as the singularity spectrum describes univocally their multi-scaling properties.

There is a long debate about the existence of universality in multiplicative processes. It is not our goal to review all the theoretical arguments that have been proposed either to favor or deny its existence; the interested reader can consult Ref. [24] and references therein. Anyway, the results shown in this paper (the coincidence between spectra within the experimental error) are compatible with the existence of multifractal universality classes.

Several aspects of our study must be remarked. The method implemented to assess and evaluate the singularity spectra has been tested previously under many different signals ranging from monofractals [42] to artificially generated data [40]

Table 3
Summary of the performance of the reconstruction formula, Eq. (11), on the six studied ensembles. To provide a stable determination of the MSM, we have defined the MSM as the 30% most singular points. The singularities were calculated with an optimized numerical implementation of the Lorentzian wavelet, as in Ref. [26,27]. The quality of the reconstruction is given by the value of the PSNR. For each ensemble, we give the minimum and maximum values of PSNR obtained for a signal in that ensemble and the average of all the values of PSNR in that ensemble.

Ensemble	A	B	C	D	E	F
Min PSNR (dB)	21.47	19.65	18.48	27.65	28.41	21.65
Max PSNR (dB)	31.36	24.72	25.40	27.85	44.78	31.91
Mean PSNR (dB)	25.74	21.56	22.35	27.75	33.40	27.86

(and therefore under absolute control). It is very stable, accurate and efficient and therefore a reliable tool to undertake multifractal signal processing [43].

The singularity spectra of our datasets have a prominent feature: there exists a finite minimum value for the singularity exponents, i.e., the spectra are bounded from below. This can be expected since we work with finite variation signals (i.e., bounded over compact sets); see discussion in Ref. [14]. Such a lower bound is incompatible with some of the models used to describe multifractal phenomena, as log-normal and the majority of log-Lévy models. Some possible candidates to fit our experimental data are log-Poisson models, including log-Poisson compound processes [52], as proposed in some models of turbulence [53–55].

There is another aspect that deserves special attention. Since one observes so-close singularity spectra in systems of a very different nature and also with different dimensionality, we are naturally led to ask whether there exists a common mechanism giving rise to multifractality. As explained in the introduction, this question is not new and has been discussed previously in the literature [24]. In the case of turbulence, it is commonly accepted that there exists a cascade process, where the energy or enstrophy flux is transferred from large to small scales, from the vertex of a hierarchy to the lower stages. It is important to realize that in the other systems we have an analogous process: recent approaches to multifractal systems [55, 44,14] identify this vertex with the Most Singular Manifold (MSM), i.e., the fractal component associated to the lowest value of singularity exponent. The MSM is a crucial ingredient in log-Poisson multifractals, as it can be used to compactly describe them [55], and even to recover the whole multifractal structure [56,44]. The big success of MMF is that it allows explicit identification of the points belonging to the MSM on real signals, from which the signals can be reconstructed with an algorithm based on the multiplicative cascade.

The reconstruction formula was first presented in Ref. [44], and has been shown to provide high-quality results in a variety of contexts [14,15,26,25,27]. The starting data in the reconstruction algorithm are the values of the gradient of the signal over the MSM only, the so-called essential gradient $\nabla_\infty s$, that is:

$$\nabla_\infty s(\vec{x}) \equiv \nabla s(\vec{x}) \delta_{F_\infty}(\vec{x}) \tag{9}$$

where $\delta_{F_\infty}(\vec{x})$ is a delta-like function with support on the MSM F_∞. The reconstruction formula is a functional $\mathcal{G}$ such that:

$$\mathcal{G}\left[\nabla_\infty s\right](\vec{x}) = s(\vec{x}) \tag{10}$$

i.e., a functional which allows retrieving the signal s from its essential gradient. As demonstrated in Ref. [44], there is only one such functional $\mathcal{G}$ which verifies the following symmetries: determinism, translational invariance, scale invariance, isotropy and compatibility with the shape of the power spectrum. All those symmetries are reasonable if the functional $\mathcal{G}$ is universal, as the known statistical symmetries of the ensembles of multifractal signals must be restored. After applying these symmetries, the reconstruction formula reads:

$$s(\vec{x}) = \left(\vec{g} \otimes \nabla_\infty s\right)(\vec{x}) \tag{11}$$

where $\otimes$ is the convolution dot product and $\vec{g}$ is the reconstruction density kernel, which has a simple expression in the Fourier space:

$$\hat{\vec{g}}(\vec{k}) = \mathrm{i}\frac{\vec{k}}{k^2}. \tag{12}$$

To conclude our analysis and as a validity check, we have applied this reconstruction algorithm to our dataset. In fact, all the signals considered in this study can be reconstructed at a great quality. In Table 3 we present a summary of the performance of the reconstruction algorithm on our 6 ensembles; see also Fig. 5 for two particular examples, as well as the ones reported in Ref. [44,14,26]. We measure the quality of the reconstruction in terms of the Peak Signal-to-Noise Ratio (PSNR): PSNR $= 10\log(\text{variance of error}/\text{dynamic range}^2)$ (expressed in dB). Some reference values of PSNR commonly used in signal processing are the following: below 20 dB: low quality reconstruction; from 20 to 30 dB: fair quality reconstruction; from 30 to 40 dB: high quality reconstruction; beyond 40 dB: almost perfect reconstruction. Our results show that our signals can be described from medium to high quality using the reconstruction algorithm, so confirming that these signals are well described as a cascade process from the MSM.

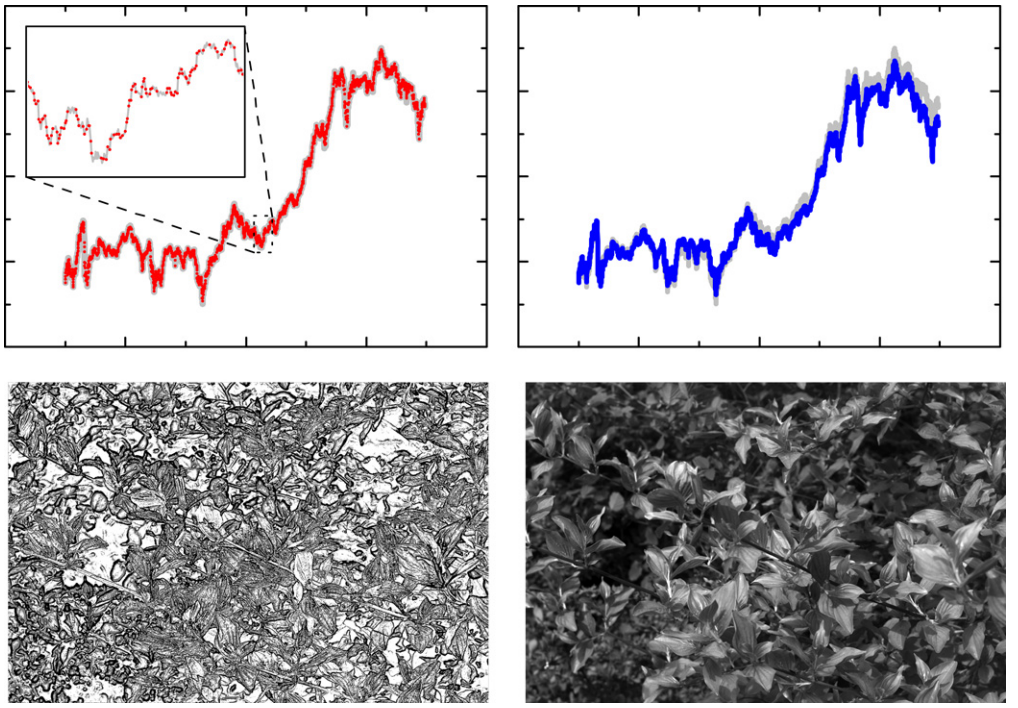

Fig. 5. Left: MSM derived from the representative signals of Ensemble A (top) and Ensemble E (bottom) shown in Fig. 1. Right: Reconstruction from the values of the gradient over the respective MSM's [44]; the quality of the reconstructions (PSNR) are 29.7 dB and 37.4 dB respectively.

5. Conclusions

The development of the microcanonical multifractal formalism has given rise to a substantial advance in the field of multifractal systems. It allows a geometrical description of the signal through local, point-wise analysis of its scaling exponents. The whole set of exponents defines the singularity spectrum, which describes the scaling properties of the system and can be used to characterize the local behavior of any functional defined on it.

In this paper, we have shown that six very different systems, ranging from Biology to Physics and passing through Economics are multifractal in the microcanonical sense of MMF. We have also shown that, within our experimental uncertainty, the singularity spectra of all the studied systems coincide. These results are compatible with the existence of a multifractal universality class that would include the systems we have studied. In this context, the most singular manifold (MSM) plays a crucial role not only because it contains the maximum amount of information about the signal but also because the MSM allows the reconstruction of the whole signal in a multiplicative sequence, analogous to the cascade process in turbulence, following a precise and well defined way. This process could explain the common shape of the singularity spectra and would be the effective microscopic mechanism giving rise to multifractality in real-world signals. New research should be addressed to understand why natural systems self-organize in a multiplicative cascade.

Applications of the MSM-based cascade process could include, e.g., devising efficient codes for image compression [44], inference of missing information in satellite data [27] and forecasting of stock market prices [14].

Acknowledgments

We are grateful to Dr. Pere Puig for his sea temperature series; these data were obtained under the EU RESPONSE project (QLRT-2001-00787). We also thank Sociedad de Bolsas for the Spanish stock market data. O. Pont is funded by a Ph.D. contract from Generalitat de Catalunya (GdC). We acknowledge financial support from MoE, contract FIS2006-13321-CO2-01, and from GdC, contract 2005SGR00889. This is a contribution to the EU MERSEA project (AIP3-CT-2003-502885) and to the Spanish projects OCEANTECH (PIF 2006) and MIDAS-4 (ESP2005-06823-C05-1).

Appendix A. Description of the data

We have used six datasets, each containing a variable number of experimental 1D and 2D signals with different amounts of sampling points. Details on their acquisition and preprocessing are the following:

- Ensemble A: 20 quotation time series from the Spanish stock market over a period of about ten years, from 1990 to 2000, sampled daily. The logarithm of the price in euros has been taken, so that derivatives correspond to relative

variations. 19 of the series belong to very liquid stocks that have been part of the Spanish composite index IBEX35 most of the analyzed period. The last series is the value of the IBEX35 index itself.

- Ensemble B: 9 currency exchange rate time series in a five-year period, from 1992 to 1997, sampled daily. The logarithm of the exchange rate has been taken, as in the ensemble A. The series correspond to exchange rates of couples obtained combining Australian Dollar, US Dollar, Euro, Japanese Yen and Swiss Franc. The 9 series are all possible couples except AUD vs. CHF.
- Ensemble C: 6 temperature time series, obtained from a mooring settled in front of the Ebro river delta by ICM scientists [45,46]. Temperature is expressed in Celsius degrees. The series were acquired at a rate of one record every three minutes during three months. The six series come from six sensors moored at depths of 25 m, 30 m, 35 m, 40 m, 45 m and 50 m. Due to device inertia and limited accuracy, the measured variations on a three-minute scale too often vanish, resulting in an apparent smoothening of the series at finer resolutions. To avoid this effect, we have downsampled the series by a factor 4.
- Ensemble D: Two weekly averages of Sea Surface Temperature images have been considered, one corresponding to the week 2 to 9 February 2003 and the other obtained for the period 14 to 21 April 2004. Temperature is expressed in Celsius degrees. On both images we have selected an area going from 34 degrees West to 8.5 degrees East in Longitude, and from 45 degrees South to 2.5 degrees South in Latitude. This corresponds to an area in the South Atlantic, which has been found rather free of missing points (i.e., points for which no acquisition was possible, mainly due to the presence of clouds). Data are available at http://oceancolor.gsfc.nasa.gov/.
- Ensemble E: 14 natural images from Hans van Hateren's web database [47]. They have been visually chosen so they have good enough contrast, because many of van Hateren's images are too dark; no further requirement has been imposed. They have been chosen among those with index number finishing in 20.[1]
- Ensemble F: 50 2D maps of high-Reynolds velocity fields generated in a wind tunnel. The velocities were estimated using the Maximum Cross Correlation Method [49] on a dispersed colorant, and expressed in cm/s. Data and methods are described in Ref. [48]. The processed signal is the modulus of the velocity vector.

References

[1] R. Benzi, G. Paladin, G. Parisi, A. Vulpiani, On the multifractal nature of fully developed turbulence and chaotic systems, Journal of Physics A 17 (1984) 3521–3531.
[2] C. Meneveau, K.R. Sreenivasan, Simple multifractal cascade model for fully developed turbulence, Physical Review Letters 59 (1987) 1424–1427, doi:10.1103/PhysRevLett.59.1424.
[3] J.F. Muzy, E. Bacry, A. Arneodo, Wavelets and multifractal formalism for singular signals: Application to turbulence data, Physical Review Letters 67 (1991) 3515–3518.
[4] K.R. Sreenivasan, Fractals and multifractals in fluid turbulence, Annual Review of Fluid Mechanics 23 (1991) 539–600.
[5] U. Frisch, Turbulence, Cambridge Univ. Press, Cambridge, MA, 1995.
[6] A. Arneodo, C. Baudet, F. Belin, R. Benzi, B. Castaing, B. Chabaud, R. Chavarria, S. Ciliberto, R. Camussi, F. Chilla, B. Dubrulle, Y. Gagne, B. Hébral, J. Herweijer, M. Marchand, J. Maurer, J.F. Muzy, A. Naert, A. Noullez, J. Peinke, F. Roux, P. Tabeling, W. vandeWater, H. Willaime, Structure functions in turbulence, in various flow configurations, at a Reynolds number between 30 and 5000, using extended self-similarity, Europhysics Letters 34 (6) (1996) 411–416.
[7] P. Kestener, A. Arnéodo, Three-dimensional wavelet-based multifractal method: The need for revisiting the multifractal description of turbulence dissipation data, Physical Review Letters 91 (19) (2003) 194501.
[8] A. Turiel, G. Mato, N. Parga, J.P. Nadal, The self-similarity properties of natural images resemble those of turbulent flows, Physical Review Letters 80 (1998) 1098–1101.
[9] A. Turiel, N. Parga, The multi-fractal structure of contrast changes in natural images: From sharp edges to textures, Neural Computation 12 (2000) 763–793.
[10] R.N. Mantegna, H.E. Stanley, Turbulence and financial markets, Nature 383 (1996) 587–588.
[11] B.B. Mandelbrot, A. Fisher, L. Calvet, A multifractal model of asset returns, Cowles Foundation Discussion Paper No. 1164, 1997.
[12] J.F. Muzy, J. Delour, E. Bacry, Modelling fluctuations of financial time series: From cascade process to stochastic volatility model, The European Physical Journal B 17 (2000) 537–548.
[13] F. Schmitt, D. Schertzer, S. Lovejoy, Multifractal fluctuations in finance, International Journal of Theoretical and Applied Finance 3 (2000) 361–364.
[14] A. Turiel, C. Pérez-Vicente, Multifractal geometry in stock market time series, Physica A 322 (2003) 629–649.
[15] A. Turiel, C. Pérez-Vicente, Role of multifractal sources in the analysis of stock market time series, Physica A 355 (2005) 475–496.
[16] P. Oswiecimka, J. Kwapien, S. Drozdz, R. Rak, Investigating multifractality of stock market fluctuations using wavelet and detrending fluctuation methods, Acta Physica Polonica B 36 (2005) 2447–2457.
[17] A. Turiel, C. Perez-Vicente, Dynamical decomposition of multifractal time series as fractal evolution and long-term cycles: Applications to foreign currency exchange market, in: Complexus Mundi: Emergent patterns in Nature, 2006, pp. 73–82.
[18] Y. Ashkenazy, J.A. Hausdorff, H.E. Stanley, P.C. Ivanov, A stochastic model of human gait dynamics, Physica A 316 (2002) 662–670.
[19] B.J. West, N. Scafetta, L. Griffin, Holder exponent spectra for human gait, Physica A 328 (2003) 561–583.
[20] L.F. Burlaga, Multifractal structure of the interplanetary magnetic field — voyager 2 observations near 25 au, 1987–1988, Geophysical Research Letters 18 (1) (1991) 69–72.
[21] R.H. Riedi, M.S. Crouse, V.J. Ribeiro, R.G. Baraniuk, A multifractal wavelet model with application to network traffic, IEEE Transactions on Information Theory 45 (4) (1999) 992–1018.
[22] S. Lovejoy, W.J.S. Curri, Y. Tessier, M.R. Claereboudt, E. Bourget, J.C. Roff, E. Schertzer, Universal multifractals and ocean patchiness: Phytoplankton, physical fields and coastal heterogeneityp, Journal of Plankton Research 23 (2) (2001) 117–141.
[23] V.K. Gupta, E.C. Waymire, A statistical analysis of mesoscale rainfall as a random cascade, Journal of Applied Meteorology 32 (1993) 251–267.

[1] The list of chosen images is the following: imk00220.imc, imk00420.imc, imk01020.imc, imk01120.imc, imk01320.imc, imk01420.imc, imk01620.imc, imk01720.imc, imk01820.imc, imk02120.imc, imk02620.imc, imk02720.imc, imk03020.imc and imk03920.imc.

[24] D. Schertzer, S. Lovejoy, Universal multifractals do exist!: Comments on a statistical analysis of mesoscale rainfall as a random cascade, Journal of Applied Meteorology 36 (1997) 1296–1303.
[25] A. Turiel, J. Grazzini, H. Yahia, Multiscale techniques for the detection of precipitation using thermal ir satellite images, IEEE Geoscience and Remote Sensing Letters 2 (4) (2005) 447–450, doi:10.1109/LGRS.2005.852712.
[26] A. Turiel, J. Isern-Fontanet, E. García-Ladona, J. Font, Multifractal method for the instantaneous evaluation of the stream function in geophysical flows, Physical Review Letters 95 (10) (2005) 104502, doi:10.1103/PhysRevLett.95.104502.
[27] J. Isern-Fontanet, A. Turiel, E. Garcia-Ladona, J. Font, Microcanonical multifractal formalism: Application to the estimation of ocean surface velocities, Journal of Geophysical Research 112 (2007) C05024.
[28] L.A.N. Amaral, A.L. Goldberger, P.Ch. Ivanov, H.E. Stanley, Scale-independent measures and pathologic cardiac dynamics, Physical Review Letters 81 (11) (1998) 2388–2391.
[29] P. Ivanov, L. Amaral, A. Goldberger, S. Havlin, M. Rosenblum, Z. Struzik, H. Stanley, Multifractality in human heartbeat dynamics, Nature 399 (1999) 461–465.
[30] Z. Neufeld, C. Lopez, E. Hernandez-Garcia, T. Tel, Multifractal structure of chaotically advected chemical fields, Physical Review E 61 (4) (2000) 3857–3866.
[31] I.J. Benczik, Z. Neufeld, T. Tél, Multifractal spectra of chemical fields in fluid flows, Physical Review E 71 (2005) 016208.
[32] S.G. Roux, A. Arneodo, N. Decoster, A wavelet-based method for multifractal image analysis. iii. applications to high-resolution satellite images of cloud structure, The European Physical Journal B 15 (2000) 765–786.
[33] D. Sachs, S. Lovejoy, D. Schertzer, The multifractal scaling of cloud radiances from 1 m to 1 km, Fractals 10 (3) (2002) 1–12.
[34] A. Davis, A. Marshak, W. Wiscombe, Wavelet based multifractal analysis of non-stationary and/or intermittent geophysical signals, in: E. Foufoula-Georgiou, P. Kumar (Eds.), Wavelets in Geophysics, Academic Press, New York, 1994, pp. 249–298.
[35] Y. Chigirinskaya, D. Schertzer, S. Lovejoy, A. Lazarev, A. Ordanovich, Unified multifractal atmospheric dynamics tested in the tropics part 1: Horizontal scaling and self organized criticality, Nonlinear Processes in Geophysics 1 (1994) 105–114.
[36] R. Benzi, S. Patarnello, P. Santangelo, Self-similar coherent structures in two-dimensional decaying turbulence, Journal of Physics A: Mathematical and General 21 (1988) 1221–1237.
[37] C. Meneveau, K.R. Sreenivasan, The multifractal nature of turbulent energy dissipation, Journal of Fluid Mechanics 224 (1991) 429–484.
[38] A. Arneodo, F. Argoul, E. Bacry, J. Elezgaray, J.F. Muzy, Ondelettes multifractales et turbulence, Diderot Editeur, Paris, France, 1995.
[39] G. Parisi, U. Frisch, On the singularity structure of fully developed turbulence, in: M. Ghil, R. Benzi, G. Parisi (Eds.), Turbulence and Predictability in Geophysical Fluid Dynamics. Proc. Intl. School of Physics E. Fermi, North Holland, Amsterdam, 1985, pp. 84–87.
[40] A. Turiel, C. Pérez-Vicente, J. Grazzini, Numerical methods for the estimation of multifractal singularity spectra on sampled data: A comparative study, Journal of Computational Physics 216 (1) (2006) 362–390.
[41] A.B. Chhabra, C. Meneveau, R.V. Jensen, K.R. Sreenivasan, Direct determination of the f(*alpha*) singularity spectrum and its application to fully developed turbulence, Physical Review A 40 (9) (1989) 5284–5294.
[42] O. Pont, A. Turiel, C.J. Pérez-Vicente, Application of the microcanonical multifractal formalism to monofractal systems, Physical Review E 74 (2006) 061110–061123.
[43] A. Turiel, H. Yahia, C. Pérez-Vicente, Microcanonical multifractal formalism: A geometrical approach to multifractal systems. Part I: Singularity analysis, Journal of Physics A 41 (2008) 015501.
[44] A. Turiel, A. del Pozo, Reconstructing images from their most singular fractal manifold, IEEE Transactions on Image Processing 11 (2002) 345–350.
[45] A. Palanques, P. Puig, J. Guillén, J. Jiménez, V. Gràcia, A. Sánchez Arcilla, O. Madsen, Near-bottom suspended sediment fluxes on a river-influenced, tideless fetch-limited shelf (the Ebro continental shelf, nw Mediterranean), Continental Shelf Research 22 (2) (2002) 285–303.
[46] P. Puig, A. Palanques, J.A. Guillén, Near-bottom suspended sediment variability caused by storms and near-inertial internal waves in the Ebro mid continental shelf (nw Mediterranean), Marine Geology 178 (1–4) (2001) 81–93.
[47] J.H. van Hateren, A. van der Schaaf, Independent component filters of natural images compared with simple cells in primary visual cortex, Proceedings of the Royal Society of London B265 (1998) 359–366.
[48] R.J. Adrian, C.D. Meinhart, C.D. Tomkins, Vortex organization in the outer region of a turbulent boundary layer, Journal of Fluid Mechanics 422 (2000) 1–53.
[49] W.J. Emery, A.C. Thomas, M.J. Collins, W.R. Crawford, D.L. Mackas, An objective method for computing advective surface velocities from sequential infrared satellite images, Journal of Geophysical Research 91 (1986) 12865–12878.
[50] K. Falconer, Fractal Geometry: Mathematical Foundations and Applications, John Wiley and sons, Chichester, 1990.
[51] H.E. Stanley, Introduction to Phase Transitions and Critical Phenomena, Oxford Science publications, Oxford, UK, 1987.
[52] B. Castaing, The temperature of turbulent flows, Journal de Physique II 6 (1996) 105–114.
[53] E.A. Novikov, Infinitely divisible distributions in turbulence, Physical Reviev E 50 (1994) R3303.
[54] B. Dubrulle, Intermittency in fully developed turbulence: Log-poisson statistics and generalized scale covariance, Physical Review Letters 73 (1994) 959–962.
[55] Z.S. She, E.C. Waymire, Quantized energy cascade and log-poisson statistics in fully developed turbulence, Physical Review Letters 74 (1995) 262–265.
[56] Z.S. She, E. Leveque, Universal scaling laws in fully developed turbulence, Physical Review Letters 72 (1994) 336–339.